ZnO Nanoparticles with Hexagonal Cone, Hexagonal Plate, and Rod Shapes: Synthesis and Characterization

Sun Young Kim, In Su Lee,† Yun Seon Yeon, Seung Min Park,* and Jae Kyu Song*

*Department of Chemistry, Kyunghee University, Seoul 130-701, Korea. *E-mail: smpark@khu.ac.kr; jaeksong@khu.ac.kr*
†College of Environment and Applied Chemistry, Kyunghee University, Gyeonggi 449-701, Korea
Received June 16, 2008

The roles of coordinating ligands (TOPO, OA, HDA, and TDPA) for the synthesis of ZnO nanoparticles are investigated. Various shapes (hexagonal cone, hexagonal plate, and rod) and sizes (5-100 nm) of ZnO nanoparticles are prepared in relation to the coordinating ligands. The hexagonal shapes (≤ 100 nm) are synthesized with TOPO and OA, while smaller size nanorods (5 × 30 nm) are with TOPO and TDPA. The relative intensities of two distinctive emission bands centered at 385 and 500 nm, which are related to the exciton and defect states, respectively, depend on the crystal qualities of ZnO nanoparticles affected by the coordinating ligands. The intense UV emissions with the reduced visible emissions are found in the monodisperse nanoparticles such as hexagonal cones and nanorods, suggesting that the monodispersity as well as the crystallinity is closely related to the coordinating ligands. The blue-shift of photoluminescence and absorption edge is observed in the nanorods, because the sizes of the nanorods are in the quantum confinement regime.

Key Words : ZnO, Nanoparticles, Coordinating ligands, Photoluminescence

Introduction

Zinc oxide (ZnO) is a direct band gap semiconductor with a band gap of 3.37 eV and an exciton binding energy of 60 meV, which promise ZnO for a candidate of optical and optoelectronic applications.[1-4] The large band gap is suitable for UV/blue emitters, while the large exciton binding energy affords stable exciton states at room temperature for efficient optical applications. In general, the photoluminescence (PL) spectrum of ZnO exhibits UV emissions from the exciton states and broad visible emissions from the defects.[5-13] The visible emissions are attributed to several types of defects such as oxygen vacancies,[5-13] because the wavelengths and the intensities of the visible emissions depend on the fabrication methods[13] and the defects have a close relationship with the growth process. Therefore, the competition between exciton and defect emissions as well as the competition between radiative and nonradiative relaxations is of importance for UV/blue ZnO optical devices. Recently, low-dimensional structures are demonstrated to have better optical properties than the bulk materials due to the large oscillator strength and the enhanced emission efficiency that originate from the quantum confinement effect.[14-18] Accordingly, a great deal of attention has been paid to nanocrystalline materials for the study of the size-dependent quantum confinement effects. However, the ZnO nanocrystals have not been investigated as much as other semiconductor nanocrystals such as CdSe despite the possibility of UV/blue applications. In this study, we present the roles of coordinating ligands for the synthesis of ZnO nanoparticles. Several sizes and shapes of nanoparticles are prepared in relation to the coordinating ligands. The relatively intense UV emissions with the reduced visible emissions are observed in the hexagonal cones and nanorods, where the nanoparticles are monodisperse. The quantum confinement effects appear clearly in the small size ZnO nanoparticles.

Experiments

Chemicals. Anhydrous zinc acetate ($ZnAc_2$, Aldrich, 99.99%), trioctylphosphine oxide (TOPO, Aldrich, 99%), octyl ether (Aldrich, 99%), 1-hexadecylamine (HDA, Aldrich, 98%), tetradecylphosphonic acid (TDPA, Alfa Aesar, 98%), oleic acid (OA, TCI, 99%), 1,12-dodecanediol (TCI, > 97%).

Synthesis. The synthesis of ZnO nanoparticles in non-hydrolytic conditions was carried out in a nitrogen atmosphere using standard Schlenk techniques, as described in other studies.[19,20] The nanoparticles were mainly synthesized by ester elimination reactions between $ZnAc_2$ and 1,12-dodecanediol in the presence of various coordinating ligands. 1,12-Dodecanediol was added to a solution of zinc-surfactant/ligand complex, which was prepared by the *in-situ* reaction between $ZnAc_2$ and ligands, and reacted by the increase of the temperature. The addition of acetone followed by the centrifugation produced white precipitates of nanoparticles. Purification of ZnO nanoparticles was carried out by the repeated dispersion in chloroform, the addition of methanol and ethanol, and the centrifugation. In order to investigate the influence of stabilizing ligands on the shape and properties of resulting nanoparticles and find the optimum synthetic conditions, several kinds of ligands, including TOPO, OA, HDA, and TDPA, were introduced.

Method I: The mixture of $ZnAc_2$ (2 mmol), TOPO (2, 4, 6, and 8 mmol), OA (0 and 10 mmol), and octyl ether was heated to 200 °C and maintained at this temperature for 1 hour. After cooling to room temperature, 1,12-dodecanediol

(12 mmol) was added and then heated to 250 °C and maintained at this temperature for 2 hours.

Method II: The mixture of $ZnAc_2$ (2 mmol) and HDA (40 mmol) was heated to 200 °C and maintained at this temperature for 1 hour. After cooling to room temperature, 1,12-dodecanediol (10 mmol) was added and then heated to 280 °C and maintained at this temperature for 2 hours.

Method III: The mixture of $ZnAc_2$ (2 mmol), TOPO (6 mmol), TDPA (1 mmol), and octyl ether was heated to 200 °C and maintained at this temperature for 1 hour. After cooling to room temperature, 1,12-dodecanediol (6 mmol) was added and then heated to 250 °C and maintained at this temperature for 2 hours.

Characterization. The synthesized nanoparticles were characterized by transmission electron microscopy (TEM, Technai 30) at an acceleration voltage of 300 kV. The TEM samples were prepared by drop coating of nanoparticles dispersed in chloroform onto a carbon-coated holey copper grid, which is followed by drying at room temperature. In order to obtain PL spectrum, nanoparticles drop-coated onto glass substrates were excited with a He-Cd laser (325 nm), which is loosely focused by a UV lens. The emission was collected at the right angle by another UV lens, spectrally resolved by a monochromator, and detected by a photomultiplier tube.

Results and Discussion

Figure 1 shows TEM images of ZnO nanoparticles prepared by TOPO and OA as stabilizing ligands as a function of the amount of TOPO, because TOPO is one of the most widely used coordinating ligands for the synthesis of nanocrystals.[21-25] When the molar ratio of TOPO to $ZnAc_2$ is 1:1, *i.e.*, $ZnAc_2$:TOPO = 1:1 (Method I), ZnO nanoparticles with an average size of ~20 nm are generated. (The TEM image of ZnO nanoparticles synthesized at the condition of 1:1 is not shown here.) The size of the prepared nanoparticles is found to increase with the increase in the amount of TOPO, resulting in the average sizes of ~40 nm (Fig. 1(a)) and ~100 nm (Fig. 1(b)) at the conditions of 1:2 and 1:3, respectively. But the sizes do not increase further beyond the molar ratio of 1:3. Thus, the nanoparticle sizes at the conditions of 1:3 are similar to those at 1:4 (Fig. 1(e)). Most of nanoparticles in Figure 1 show hexagonal morphology regardless of the sizes, supporting that ZnO favors the wurtzite structures, although the detailed shapes of the nanoparticles are not identical. For example, the nanoparticles at the condition of 1:3 are hexagonal cone shapes, as shown by the magnified TEM images in Figure 1(c) and 1(d), while hexagonal plate shapes are found at 1:2 and 1:4. We note that the hexagonal cone shapes are observed only at the condition of 1:3, where the nanoparticles are in the most monodisperse sizes. These observations suggest a facile route to control the size and shape of the ZnO nanoparticles simply by changing the molar ratio of the ligand (TOPO) to the metal precursor ($ZnAc_2$), although the detailed mechanism for the dependence on the molar ratio needs further investigations.

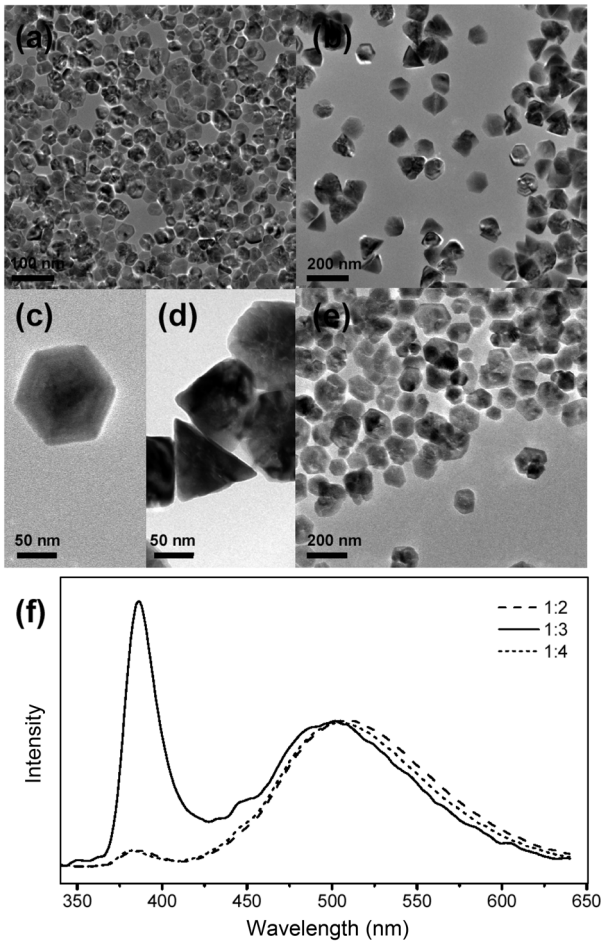

Figure 1. (a) The TEM image of ZnO nanoparticles prepared by Method I ($ZnAc_2$:TOPO = 1:2). (b) The TEM image of ZnO nanoparticles prepared by Method I ($ZnAc_2$:TOPO = 1:3). (c) (top view) The magnified TEM image presents a hexagonal shape of ZnO nanoparticle ($ZnAc_2$:TOPO = 1:3). (d) (side view) The magnified TEM image presents a cone shape of ZnO nanoparticle ($ZnAc_2$:TOPO = 1:3). (e) The TEM image of ZnO nanoparticles prepared by Method I ($ZnAc_2$:TOPO = 1:4). (f) Photoluminescence spectra of ZnO nanoparticles prepared by Method I. The molar ratios of TOPO to $ZnAc_2$ are presented in the inset, *i.e.*, $ZnAc_2$:TOPO = 1:2, 1:3, and 1:4.

Photophysical properties of the synthesized nanoparticles are investigated by PL measurements. All nanoparticles show two distinctive emission bands centered at 385 and 500 nm (Figure 1(f)). The UV emissions at 385 nm result from the exciton recombinations of the ZnO nanoparticles, while the visible emissions at 500 nm are from the defects such as the oxygen vacancies.[5-13] Interestingly, the nanoparticles at the condition of 1:3, where the monodisperse size distributions are observed by TEM images, show the reduced visible emissions compared to the UV emissions, suggesting good crystal quality of the nanoparticles, *i.e.*, a low defect density in the nanoparticles. We note that the competition between UV and visible emissions is crucial for the applications of ZnO nanoparticles as optically active media, because the advantage of ZnO lies in its large band gap. Therefore, the relatively intense UV emissions of the

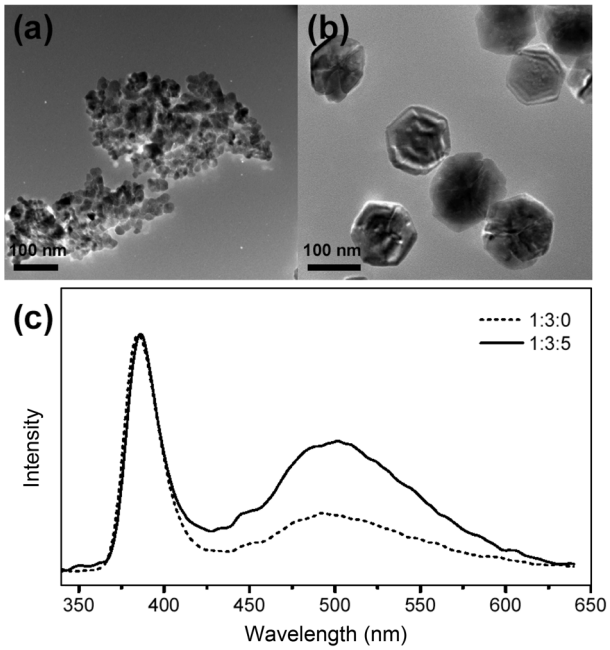

Figure 2. (a) The TEM image of ZnO nanoparticles prepared by Method I without OA ($ZnAc_2$:TOPO:OA = 1:3:0). (b) The TEM image of ZnO nanoparticles prepared by Method I with OA ($ZnAc_2$:TOPO:OA = 1:3:5). (c) Photoluminescence spectra of ZnO nanoparticles prepared by Method I by changing the molar ratio of OA. The molar ratios of OA to $ZnAc_2$ and TOPO are presented.

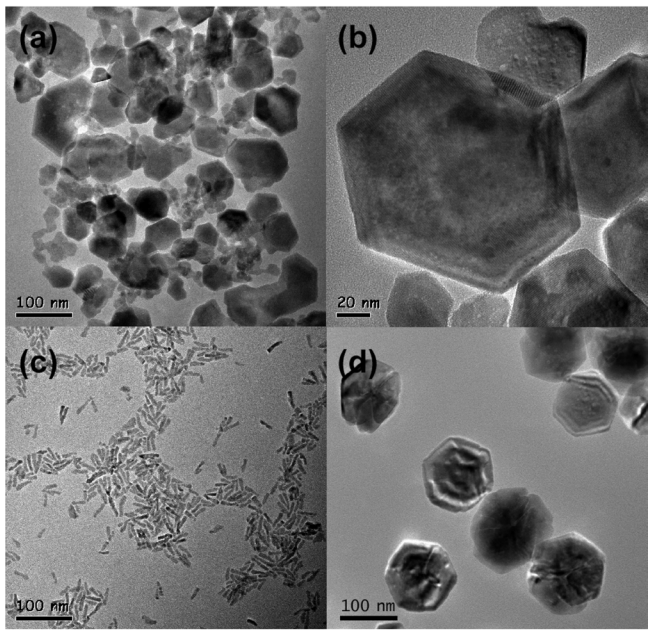

Figure 3. (a) The TEM image presents the hexagonal plate shapes of ZnO nanoparticles prepared by Method II. (b) The magnified TEM image (Method II) presents a clear view of the hexagonal shapes of ZnO nanoparticles. (c) The TEM image presents the nanorod shapes of ZnO nanoparticles prepared by Method III. (d) The TEM image presents the hexagonal cone shapes of ZnO nanoparticles prepared by Method I.

hexagonal cone shapes (at the condition of 1:3) demonstrate the importance of the suitable molar ratio of the coordinating ligands.

The roles of OA as co-coordinating ligands are studied by changing the molar ratio of OA (Method I). Figure 2 shows the selected TEM images of nanoparticles obtained by changing the molar ratio of OA with other parameters unchanged ($ZnAc_2$:TOPO = 1:3). In the absence of OA, smaller size nanoparticles are aggregated possibly due to insufficient capping functions of OA. However, as discussed above, nearly monodisperse nanoparticles of larger sizes are prepared in the presence of OA. The control experiments by keeping other reaction parameters unchanged show that OA also plays an important role in the formation of the monodisperse nanoparticles. In the PL spectra in Figure 2(c), on the other hand, the defect emissions around 500 nm are less dominant in the aggregated nanoparticles. Since the oxygen vacancies are the candidates for the recombination centers of the visible emissions and the oxygen vacancies are mainly located on the surface,[5-13] the surface-to-volume ratio are at play for the competition of UV and visible emissions. Therefore, the reduced visible emissions seem to be related to smaller surface-to-volume ratio, despite seemingly smaller sizes of the composite nanoparticles, mainly due to the aggregation of nanoparticles.

In addition, the roles of other coordinating ligands such as HDA and TDPA are investigated, because HDA and TDPA are well-known coordinating ligands for the synthesis of nanoparticles.[21-25] Although HDA is found as the best primary amines generating the nanoparticles with highly efficient PL in the previous study,[24] the sizes of ZnO nanoparticles are not observed to be monodisperse in several synthesis conditions (Method II), while most of them are hexagonal plates (Fig. 3(a) and 3(b)). On the other hand, when TDPA is employed instead of OA, *i.e.*, TDPA and TOPO are the coordinating ligands (Method III), relatively monodisperse nanorods with an average size of 5 nm (thickness) × 30 nm (length) are found, as shown in Figure 3(c). This size is much smaller than other nanoparticles synthesized in this study.

In order to investigate the size-dependent photophysical properties of ZnO nanoparticles shown in Figure 3, PL spectra are obtained (Fig. 4(a)). The emission peak of the hexagonal plates (Method II) in UV region is slightly blue-shifted compared to the hexagonal cones (Method I). In addition, the emission peak of the nanorods (Method III) is further blue-shifted, which is due to quantum confinement effects. When the dimension of nanoparticles is comparable to a Bohr radius of ZnO exciton (2.34 nm),[16] the band gap increases. The relationship between band gap and size of nanoparticles are obtained by several models.[26-30] With the effective mass model for spherical particles,[26] the band gap, $E_g(r)$, can be approximated as

$$E_g(r) = E_g^{bulk} + \frac{\hbar^2 \pi^2}{2er^2}\left(\frac{1}{m_e} + \frac{1}{m_h}\right) \quad (1)$$

where E_g^{bulk} is the band gap of the bulk, r is the particle radius, m_e is the effective mass of the electrons, m_h is the effective mass of the holes, and e is the charge of the

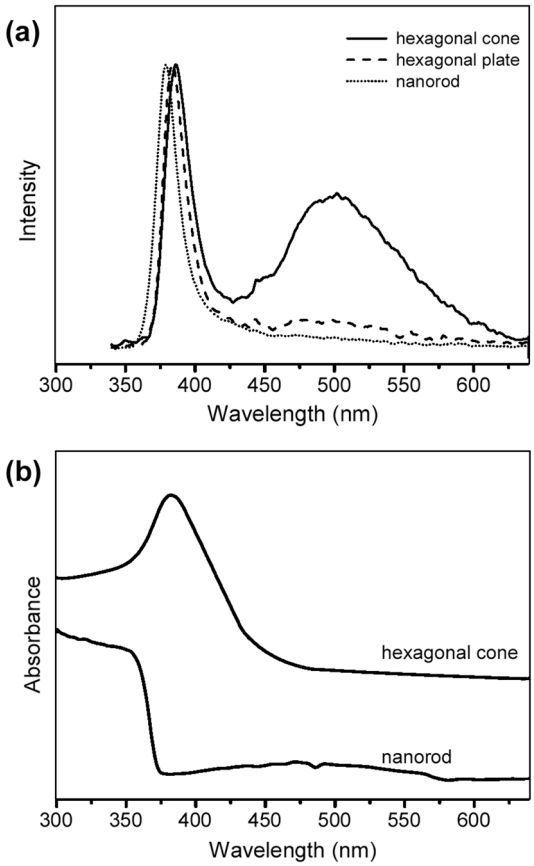

Figure 4. (a) Photoluminescence spectra of the ZnO nanoparticles prepared by Method I, II, and III. The hexagonal cone, hexagonal plate, and nanorod are prepared by Method I, II, and III, respectively. (b) Absorption spectra of the ZnO nanoparticles prepared by Method I and III. The hexagonal cone and nanorod are prepared by Method I and III, respectively.

electron. Because the hexagonal plates and the nanorods investigated in this study are not spherical shapes, it is not easy to estimate the exact band gap. However, the blue-shift of the emission (6 nm, 0.05 eV, 400 cm^{-1}) compared to the hexagonal cones seems to agree with other theoretical and experimental results.[17,30] The blue-shift of the emission peaks supports that UV emissions are related to the exciton recombinations rather than other possible processes in the ZnO nanoparticles.[5-13] We note that the broad green emissions observed in the hexagonal cones and hexagonal plates are virtually negligible in the nanorods. The absence of the visible emission suggests the good crystal quality of the nanorods.

For further investigations of the band gap variation related to the quantum confinement effects, the absorption spectra of nanoparticles are obtained. The blue-shift of absorption edge in the nanorods is observed in Figure 4(b), which is also due to the quantum confinement effects. However, when the absorption edge of the nanorods is compared to that of the hexagonal cones, the blue-shift is estimated to be 16 nm (0.14 eV, 1100 cm^{-1}). Thus, the blue-shift of the nanorods in the absorption spectrum (0.14 eV) is much larger than that in the PL spectrum (0.05 eV), when it is compared to the hexagonal cones. This distinct blue-shift seems to be related to the size-dependent Stokes shift, which is observed in other semiconductor nanoparticles such as InP and CdSe.[31] The size-dependent electron-phonon processes and spin-orbit exchange interactions are suggested to be responsible for the size-dependent Stokes shift,[31,32] although the origin in ZnO nanoparticles is not clear at present.[33]

Since the absorption to the exciton states in a single nanocrystal is spectrally narrow and depends strongly on the nanoparticle sizes, the width of the exciton absorption peak provides another measure of the size distribution in the nanoparticles. In the absorption spectrum of the nanorods (Fig. 4(b)), the characteristic exciton absorption peak is not clearly observed. Despite the seemingly similar sizes in TEM images (Fig. 3(c)), the broad absorption to the exciton states seems to indicate the size-heterogeneities. Because the band gap variation, which is closely related to the exciton states,[34] is drastic in the small size nanoparticles,[26-30] the slight heterogeneity in the small size nanoparticles results in a large change of the absorption wavelength of the exciton. Accordingly, the width of the exciton absorption peaks can be broadened significantly even with a slight heterogeneity in the regime of the strong quantum confinement effects. On the other hand, the exciton absorption peak appears clearly in the hexagonal cones (Fig. 4(b)). However, we note that it does not necessarily indicate the size homogeneity, because the band gap variation in the large size particles is hardly expected as a function of the nanoparticle size. Another thing to be noted is the slow onset of the absorption peak near the band gap in the hexagonal cones, which originates from the defect-related absorption, because the non-negligible amount of the defects are found in the PL spectrum of the hexagonal cones. On the other hand, a slow onset is not observed in the absorption spectrum of the nanorods, where the defect-related emissions are nearly absent in the PL spectrum.

Summary

We have investigated the synthesis of ZnO nanoparticles in the presence of the various coordinating ligands such as TOPO, OA, HDA, and TDPA. The hexagonal cone shapes are observed with the specific molar ratio of TOPO to $ZnAc_2$ in the presence of OA, where the nanoparticle sizes are monodisperse, implying that the hexagonal cone shape can be the stable structures in the large size regime of ZnO. When TDPA is employed as co-coordinating ligands with TOPO, much smaller size nanorods are prepared, suggesting that TDPA provides a favorable condition for the rod shapes in the small size regime of ZnO. The nanoparticles show the UV and visible emissions, which indicates the crystallinity and provides complementary information to the results obtained by TEM images. The relatively intense UV emissions compared to the visible emissions in the hexagonal cones and nanorods indicates the good crystal quality, which agrees with the roles of the coordinating ligands. The blue-shift of photoluminescence and absorption edge is observed

in the small size nanoparticles such as the nanorods, when the sizes of the nanoparticles are in the quantum confinement regime.

Acknowledgments. This work was supported by the Kyung Hee University Research Fund in 2006 (KHU-20060445).

References

1. Huang, M. H.; Mao, S.; Feick, H.; Yan, H.; Wu, Y.; Kind, H.; Weber, E.; Russo, R.; Yang, P. *Science* **2001**, *292*, 1897.
2. Cao, H.; Xu, J. Y.; Zhang, D. Z.; Chang, S.-H.; Ho, S. T.; Seeling, E. W.; Liu, X.; Chang, R. P. H. *Phys. Rev. Lett*. **2000**, *84*, 5584.
3. Tsukazaki, A.; Ohtomo, A.; Onuma, T.; Ohtani, M.; Makino, T.; Sumiya, M.; Ohtani, K.; Chichibu, S. F.; Fuke, S.; Segawa, Y.; Ohno, H.; Koinuma, H.; Kawasaki, M. *Nat. Mater*. **2005**, *4*, 42.
4. Troys, C. T. *Photonics Spectra* **1997**, *31*, 34.
5. Kang, H. S.; Kang, J. S.; Kim, J. W.; Lee, S. Y. *J. Appl. Phys*. **2004**, *95*, 1246.
6. Studenikin, S. A.; Golego, N.; Cocivera, M. *J. Appl. Phys*. **1998**, *84*, 2287.
7. Vanheusden, K.; Seager, C. H.; Warren, W. L.; Tallant, D. R.; Voigt, J. A. *Appl. Phys. Lett*. **1996**, *68*, 403.
8. Wu, L.; Wu, Y.; Pan, X.; Kong, F. *Opt. Mater*. **2006**, *28*, 418.
9. Zhang, S. B.; Wei, S. H.; Zunger, A. *Phys. Rev. B* **2001**, *63*, 075205.
10. Tuomisto, F.; Saarinen, K.; Look, D. C.; Farlow, G. C. *Phys. Rev. B* **2005**, *72*, 085206.
11. Reynolds, D. C.; Look, D. C.; Jogai, B. *J. Appl. Phys*. **2001**, *89*, 6189.
12. Guo, B.; Qiu, Z. R.; Wong, K. S. *Appl. Phys. Lett*. **2003**, *82*, 2290.
13. Li, D.; Leung, Y. H.; Djurisic, A. B.; Liu, Z. T.; Xie, M. H.; Shi, S. L.; Xu, S. J.; Chan, W. K. *Appl. Phys. Lett*. **2004**, *85*, 1601.
14. Rossi, F.; Goldoni, G.; Molinari, E. *Phys. Rev. Lett*. **1997**, *78*, 3527.
15. Choi, H.-W.; Woo, H.-J.; Kim, J.-K.; Kim, G.-D.; Hong, W.; Ji, Y.-Y. *Bull. Korean Chem. Soc*. **2004**, *25*, 525.
16. Senger, R. T.; Bajaj, K. K. *Phys. Rev. B* **2003**, *68*, 45313.
17. Gu, Y.; Kuskovsky, I. L.; Yin, M.; O'Brien, S.; Neumark, G. F. *Appl. Phys. Lett*. **2004**, *85*, 3833.
18. Hsu, W.-T.; Lin, K.-F.; Hsieh, W.-F. *Appl. Phys. Lett*. **2007**, *91*, 181913.
19. Joo, J.; Kwon, S. G.; Yu, J. H.; Hyeon, T. *Adv. Mater*. **2005**, *17*, 1873.
20. Cozzoli, P. D.; Curri, M. L.; Agostiano, A.; Leo, G.; Lomascolo, M. *J. Phys. Chem. B* **2003**, *107*, 4756.
21. Talapin, D. V.; Rogach, A. L.; Kornowski, A.; Haase, M.; Weller, H. *Nanolett*. **2001**, *1*, 207.
22. Qu, L.; Peng, A.; Peng, X. *Nanolett*. **2001**, *1*, 333.
23. Qu, L.; Peng, X. *J. Am. Chem. Soc*. **2001**, *124*, 2049.
24. Mekis, I.; Talapin, D. V.; Kornowski, A.; Haase, M.; Weller, H. *J. Phys. Chem. B* **2003**, *107*, 7454.
25. Wu, D.; Kordesch, M. E.; Van Patten, P. G. *Chem. Mater*. **2005**, *17*, 6436.
26. Brus, L. E. *J. Chem. Phys*. **1984**, *80*, 4403.
27. Hyberstsen, M. S. *Phys. Rev. Lett*. **1994**, *72*, 1514.
28. Efros, A. L.; Rosen, M. *Annu. Rev. Mater. Res*. **2000**, *30*, 475.
29. Andersen, K. E.; Fong, C. Y.; Pickett, W. E. *J. Non Cryst. Solids* **2002**, *299*, 1105.
30. Fu, Z. D.; Cui, Y. S.; Zhang, S. Y.; Chen, J.; Yu, D. P.; Zhang, S. L.; Niu, L.; Jiang, J. Z. *Appl. Phys. Lett*. **2007**, *90*, 263113.
31. Fu, H.; Zunger, A. *Phys. Rev. B* **1997**, *56*, 1496.
32. Nirmal, M.; Norris, D. J.; Kuno, M.; Bawendi, M. G.; Efros, Al. L.; Rosen, M. *Phys. Rev. Lett*. **1995**, *75*, 3728.
33. Lin, K.-F.; Cheng, H.-M.; Hsu, H.-C.; Lin, L.-J.; Hsieh, W.-F. *Chem. Phys. Lett*. **2005**, *409*, 208.
34. Kim, S. Y.; Yeon, Y. S.; Park, S. M.; Kim, J. H.; Song, J. K. *Chem. Phys. Lett*. **2008**, *462*, 100.